ISSN 1070-3284, Russian Journal of Coordination Chemistry, 2014, Vol. 40, No. 5, pp. 304–313. © Pleiades Publishing, Ltd., 2014.

# Construction of 0D to 3D Copper(II) MOFs Based on Heterocyclic Carboxylic Acid: Synthesis, Structures, Cyclic Voltammograms, and Luminescent Properties[1]

**H. M. Zhang, Q. Q. You, L. Z. Wu, L. Liu, and L. R. Yang***

*Henan Key Laboratory of Polyoxometalate, Institute of Molecule and Crystal Engineering, College of Chemistry and Chemical Engineering, Henan University, Kaifeng, 475004 P.R. China*

**e-mail: lirongyang@163.com*

Received May 16, 2013

**Abstract**—The crystal structures of MOFs $[Cu(PDA)(Phen)(H_2O)]_2 \cdot 5H_2O$ (**I**) and $[Cu(PZCA)_2(H_2O)_2] \cdot 2H_2O$ (**II**) ($H_2PDA$ = pyridine-2,6-dicarboxylic acid, Phen = 1,10-phenanthroline, HPZCA = pyrazine-2-carboxylic acid, $H_2PZDA$ = pyrazine-2,3-carboxylic acid) have been prepared under hydrothermal conditions. These MOFs have been characterized by element analysis, single-crystal X-ray diffraction, thermogravimetric analyses and IR spectroscopy. 3D frameworks of MOFs **I** and **II** are fabricated from zero-dimensional (0D) motifs through hydrogen bonds and π–π interactions. In MOF **II**, the PZCA ligand comes from in situ decarboxylation of the part of pyrazine-2,3-dicarboxylic acid ($H_2PZDA$). Luminescent emissions bands of MOF **I** in methanol have been measured at room temperature and it displays selectivity to $Zn^{2+}$, $Cu^{2+}$, $Pb^{2+}$, and $Cd^{2+}$ ions. Cyclic voltammetry of MOFs **I** and **II** showed that the Cu(II/I) couple is irreversible.

**DOI:** 10.1134/S1070328414040125

## INTRODUCTION

In recent years, the design and synthesis of metal-organic-frameworks (MOFs) structures have received enormous attention, because of their novel and potential applications in host guest chemistry, catalysis, electrochemical, luminescent and magnetism [1–6]. MOFs assembly based on the molecular building block method which has been introduced as a suitable method to design and construct these kinds of materials [7]. In light of that, many new organic ligands contribute to the occurrence of the varieties of novel polymers. Some multidentate carboxylic acid ligands containing N and O donor atoms have been widely used to assemble MOFs [8–10]. One feasible strategy involving the use of multicarboxylate ligands as the organic building block, such as pyridine-2,6-dicarboxylic acid ($H_2PDA$) and pyrazine-2,3-dicarboxylic acid ($H_2PZDA$) and their deprotonated anions ($HPDA^-$, $PDA^{2-}$, $HPZDA^-$, and $PZDA^{2-}$ tuned under appropriate pH value) adopt flexible, multidentate coordination sites, and therefore may potentially provide various coordination modes which are in favor of the construction of higher-dimensional MOFs frameworks [8, 11–16]. Herein, we have focused on developing the rational design and synthesis of this kind of frameworks.

The present paper is to report the hydrothermal synthesis, characteristics, electrochemical results, thermal analysis and the crystal structures of the 3D coordination polymers of Cu(II) connected by hydrogen bonds and π–π stacking—$[Cu(PDA)(Phen)(H_2O)]_2 \cdot 5H_2O$ (**I**) and $[Cu(PZCA)_2(H_2O)_2] \cdot 2H_2O$ (**II**). Emission spectra of MOF **I** in the presence of $Cd^{2+}$, $Cu^{2+}$, $Mg^{2+}$, $Pb^{2+}$, and $Zn^{2+}$ ions have been studied and compared with those of the assynthesized MOFs.

## EXPERIMENTAL

**Reagents and general techniques.** All chemicals are analytical grade and used without further purification. Elemental analyzer was performed on a Perkin-Elmer 240C elemental analyzer. Infrared spectra were recorded in the 4000–400 $cm^{-1}$ region using KBr pellets on an AVATAR 360FT-IR spectrometer, the crystal structure was determined on a Bruker Smart CCD X-ray single-crystal diffractometer. Fluorescent data were collected on F-7000 FL Spectrophotometer at room temperature. The TG and DTG experiment were performed using a PerkinElmer TGA7 thermogravimeter. The heating rate was programmed to be 10 K $min^{-1}$ with the protecting stream of $N_2$ owing at 40 mL $min^{-1}$. Cyclic voltammograms were obtained on a CHI650 electrochemical analyzer at 25°C.

**Synthesis of MOF I.** A mixture of $Cu(Ac)_2 \cdot H_2O$ (59.90 mg, 0.3 mmol), $H_2PDA$ (50.11 mg, 0.3 mmol),

[1] The article is published in the original.

Phen (54.02 mg, 0.3 mmol) and water (10 mL) was homogenized by stirring for 30 min, then transferred into 25 mL Teflon-lined stainless steel autoclave under autogenous pressure at 150°C for 96 h. The reaction system was cooled to room temperature and then left at room temperature for 21 days. Blue prism crystals of MOF **I** suitable for X-ray diffraction analysis were obtained with a yield of 78.6%.

For $C_{38}H_{36}N_6O_{15}Cu_2$

| | | | |
|---|---|---|---|
| anal. calcd., %: | C, 48.31; | H, 3.81; | N, 8.90. |
| Found, %: | C, 49.04; | H, 3.45; | N, 8.56. |

IR spectrum (ν, $cm^{-1}$): 3424 b, 3091 w, 3013 w, 1622 s, 1590 s, 1519 m, 1426 s, 1364 s, 1275 m, 1147 w, 1110 w, 1068 w, 1033 w, 912 w, 857 m, 812 w, 778 w, 722 s, 690 w, 647 w, 448 w, 405 w.

**Synthesis of MOF II.** A mixture of $Cu(Ac)_2 \cdot H_2O$ (59.90 mg, 0.3 mmol), $H_2PZDA$ (50.4 mg, 0.3 mmol), and water (10 mL) was homogenized by stirring for 30 min, then transferred into 25 mL Teflon-lined stainless steel autoclave under autogenous pressure at 150°C for 96 h. After cooling the reaction system to room temperature, blue prism crystals of **II** suitable for X-ray diffraction analysis were isolated with a yield of 49.1%.

For $C_{10}H_{14}N_4O_8Cu$

| | | | |
|---|---|---|---|
| anal. calcd., %: | C, 31.43; | H, 3.66; | N, 14.67. |
| Found, %: | C, 31.02; | H, 3.24; | N, 14.98. |

IR spectrum (ν, $cm^{-1}$): 3450 b, 1636 s, 1600 s, 1572 m, 1475 w, 1450 w, 1414 s, 1363 s, 1292 s, 1269 w, 1176 m, 1159 m, 1101 w, 1032 w, 863 m, 796 m, 771 w, 711 s, 699 w, 661 w, 609 w, 458 w.

**X-ray crystallographic determination.** Single-crystal diffraction data **I** and **II** were collected suitable single crystals of the MOF on a Bruker Smart CCD X-ray single-crystal diffractometer with graphite monochromated Mo$K_\alpha$-radiation (λ = 0.71073 Å) at 296(2) K. All independent reflections were collected in a range of 2.25°–25.00° for MOF **I** and 3.02°–24.98° for MOF **II** (determined in the subsequent refinement). Multi-scan empirical absorption corrections were applied to the data using the SADABS [17]. The crystal structure was solved by direct methods and Fourier synthesis. Positional and thermal parameters were refined by the full-matrix least-squares method on $F^2$ using the SHELXTL software package [18]. The final least-square cycle of refinement gave $R_1 = 0.0275$, $wR_2 = 0.0770$ for **I** and $R_1 = 0.0300$, $wR_2 = 0.0790$ for **II**, the weighting scheme $w = 1/[\sigma^2(F_o^2) + (0.0429P)^2 + 0.55P]$ for MOF **I** and $w = 1/[\sigma^2(F_o^2) + (0.0306P)^2 + 0.67P]$ for MOF **II**, where $P = (F_o^2 + 2F_c^2)/3$. A summary of the key crystallographic information is given in Table 1. Selected bond lengths and band angles for the MOFs **I** and **II** are listed in Table 2.

Supplementary material for the MOFs **I** and **II** has been deposited with the Cambridge Crystallographic Data Centre (nos. 826477 (**I**), 827162 (**II**); deposit@ccdc.cam.ac.uk or http://www.ccdc.cam.ac.uk).

## RESULTS AND DISCUSSION

MOFs **I** and **II** are stable in the solid state upon exposure to air and insoluble in common solvents, such as $CH_3COCH_3$, $CH_3CH_2OH$, $CHCl_3$, $CHCl_2$, $CH_3CN$, THF or DMF, but they are soluble in DMSO and $CH_3OH$. The solid state properties of the two MOFs were examined by IR spectra and recorded in the range of 4000–400 $cm^{-1}$ suggest that the $PDA^{2-}$, Phen (MOF **I**) and PZCA (MOF **II**) ligands coordinated to the central $Cu^{2+}$ ions. The IR spectra of the MOFs show a broad band at 3424 $cm^{-1}$ for MOF **I** and 3450 $cm^{-1}$ for MOF **II** due to the OH groups of water molecules. Strong absorption bands in the ranges 1622–1519 $cm^{-1}$ (**I**) and 1636–1572 $cm^{-1}$ (**II**) correspond to $COO^-$ vibrations groups of the $PDA^{2-}$ and PZCA ligands [9]. Two strong bands are observed at 1426, 1364 $cm^{-1}$ (**I**) and 1414, 1363 $cm^{-1}$ (**II**) that corresponds to the C–O vibration of the $PDA^{2-}$ and PZCA ligands [19, 20], respectively. The absence of the characteristic bands around 1700 $cm^{-1}$ indicates that the $H_2PDA$ and PZCA ligands of MOFs **I** and **II** are completely deprotonated in the form of $PDA^{2-}$ and $PZCA^-$ anions upon reaction with the metal ions. The weak bands 405 to 690 $cm^{-1}$ (**I**) and 458 to 699 $cm^{-1}$ (**II**) may be ascribed to Cu–N and Cu–O stretching vibrations. The conclusions above all are supported by the results obtained by X-ray diffraction measurements [21].

The unit of MOF **I** consists of two six-coordinated Cu(II) atoms, two independent $PDA^{2-}$ ligands, two Phen ligands and two coordinated water molecules (Fig. 1a). The independent $Cu^{2+}$ ions present a distorted octahedral geometry. The equatorial sites of the polyhedron are occupied by N(1) donor sets from $PDA^{2-}$, N(2), N(3) from Phen donor and O(1*w*), while the axial vertexes are occupied by O(2) and O(3) from $PDA^{2-}$. The average distances of Cu(1)–O(2) and Cu(1)–O(3) (O(2) and O(3) belonging to $PDA^{2-}$ ligand) is 2.312 Å, which is markedly longer than that of Cu(1)–O(1*w*) (2.029(15) Å). The bond length of Cu(1)–N(1) (1.988(17) Å) is slightly shorter than the average bond length (2.028 Å) of Cu(1)–N(2) and Cu(1)–N(3) (N(2) and N(3) deriving from Phen ligand), suggesting that the tridentate chelating effect of $PDA^{2-}$ ligand is more stronger than that of Phen ligand. The lengths of Cu–N, Cu–O and Cu–O(W) are consistent with those in the similar MOFs reported [4, 5]. The adjacent 0D units are connected by the hydrogen bonds (O(5*w*)–H(5*wB*)···O(8)$^{\#6}$, O(7*w*)–H(7*wA*)···O(5*w*)$^{\#1}$, O(4*w*)–H(4*wA*)···O(7*w*) and

**Table 1.** Crystallographic data and experimental details for MOFs **I** and **II**

| Parameter | Value | |
|---|---|---|
| | **I** | **II** |
| Formula weight | 943.81 | 381.79 |
| Crystal system | Triclinic | Monoclinic |
| Space group | $P\bar{1}$ | $P2_1/c$ |
| $a$, Å | 10.0603(13) | 6.9088(5) |
| $b$, Å | 13.8635(18) | 14.1990(11) |
| $c$, Å | 14.2575(19) | 8.2807(6) |
| α, deg | 97.601(2) | 90 |
| β, deg | 97.724(2) | 112.435 |
| γ, deg | 98.103(2) | 90 |
| $Z$ | 2 | 2 |
| Volume, Å$^3$ | 1927.5(4) | 750.84(10) |
| $\rho_{calcd}$, mg m$^{-3}$ | 1.626 | 1.689 |
| $F$(000) | 968 | 390 |
| Crystal size, mm | 0.48 × 0.40 × 0.28 | 0.48 × 0.44 × 0.35 |
| θ Range for data collection, deg | 2.25–25.00 | 3.02–24.98 |
| Limiting indices | $-8 \le h \le 11$, $-16 \le k \le 16$, $-16 \le l \le 16$ | $-8 \le h \le 8$, $-15 \le k \le 16$, $-5 \le l \le 9$ |
| Reflections collected/unique | 9835/6707 | 3731/1314 |
| $R_{int}$ | 0.0108 | 0.0118 |
| Data/restraints/parameters | 6707/0/550 | 1314/0/106 |
| Goodness-of-fit on $F^2$ | 1.072 | 1.139 |
| Final $R$ indices ($I > 2\sigma(I)$) | $R_1 = 0.0275$ $wR_2 = 0.0770$ | $R_1 = 0.0300$ $wR_2 = 0.0790$ |
| $R$ indices (all data) | $R_1 = 0.0333$ $wR_2 = 0.0788$ | $R_1 = 0.0326$ $wR_2 = 0.0801$ |
| Largest diff. peak and hole, $e$ Å$^{-3}$ | 0.257 and –0.300 | 0.290 and –0.277 |

**Table 2.** Selected bond lengths (Å) and band angles (deg) for the MOFs **I** and **II**

| Bond | *d*, Å | Bond | *d*, Å |
|---|---|---|---|
| | | **I** | |
| Cu(1)–N(1) | 1.9881(17) | Cu(2)–O(2*w*) | 2.0019(14) |
| Cu(1)–N(3) | 2.0032(18) | Cu(2)–N(4) | 2.0043(17) |
| Cu(1)–O(1*w*) | 2.0292(15) | Cu(2)–N(5) | 2.0096(17) |
| Cu(1)–N(2) | 2.0529(18) | Cu(2)–N(6) | 2.0515(17) |
| Cu(1)–O(2) | 2.3090(16) | Cu(2)–O(7) | 2.2535(16) |
| Cu(1)–O(3) | 2.3155(15) | Cu(2)–O(6) | 2.3500(15) |
| | | **II** | |
| Cu(1)–O(1) | 1.9549(17) | Cu(1)–N(1) | 1.9817(19) |
| Cu(1)–O(1*w*) | 2.5207(23) | | |
| Angle | ω, deg | Angle | ω, deg |
| | | **I** | |
| N(1)Cu(1)N(3) | 172.29(7) | O(2*w*)Cu(2)N(4) | 94.89(6) |
| N(1)Cu(1)O(1*w*) | 94.20(6) | O(2*w*)Cu(2)N(5) | 90.39(7) |
| N(3)Cu(1)O(1*w*) | 90.40(7) | N(4)Cu(2)N(5) | 174.70(7) |
| N(1)Cu(1)N(2) | 94.93(7) | O(2*w*)Cu(2)N(6) | 170.82(7) |
| N(3)Cu(1)N(2) | 81.21(7) | N(4)Cu(2)N(6) | 93.40(7) |
| O(1*w*)Cu(1)N(2) | 169.06(7) | N(5)Cu(2)N(6) | 81.30(7) |
| N(1)Cu(1)O(2) | 75.97(6) | O(2*w*)Cu(2)O(7) | 90.35(6) |
| N(3)Cu(1)O(2) | 97.80(6) | N(4)Cu(2)O(7) | 76.93(6) |
| O(1*w*)Cu(1)O(2) | 90.90(6) | N(5)Cu(2)O(7) | 103.55(7) |
| N(2)Cu(1)O(2) | 97.15(6) | N(6)Cu(2)O(7) | 95.37(6) |
| N(1)Cu(1)O(3) | 75.86(6) | O(2*w*)Cu(2)O(6) | 90.39(6) |
| N(3)Cu(1)O(3) | 110.52(7) | N(4)Cu(2)O(6) | 74.60(6) |
| O(1*w*)Cu(1)O(3) | 88.22(6) | N(5)Cu(2)O(6) | 104.95(6) |
| N(2)Cu(1)O(3) | 88.17(6) | N(6)Cu(2)O(6) | 88.01(6) |
| O(2)Cu(1)O(3) | 151.67(6) | O(7)Cu(2)O(6) | 151.48(5) |
| | | **II** | |
| O(1)Cu(1)N(1) | 83.36(8) | | |

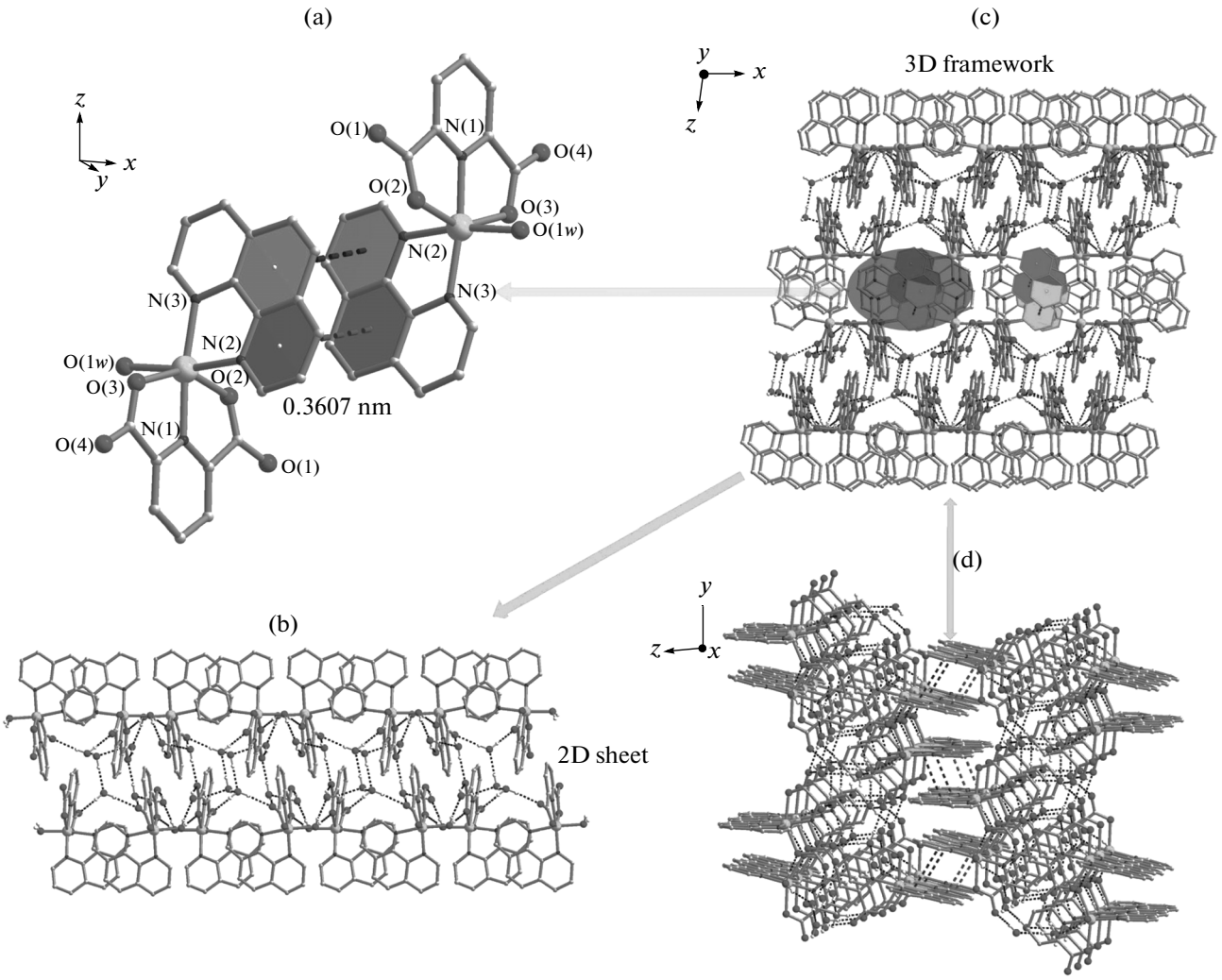


**Fig. 1.** The formation of 3D framework of $[Cu(PDA)(Phen)(H_2O)]_2 \cdot 5H_2O$: coordination environment of the MOF **I** and the π–π interactions in the MOF (a); view of the 1D chain and 2D single layer (b); view of the 3D framework in the *y* axis direction (c); view of the 3D framework in the *x* axis direction (d).

O(4*w*)–H(4*w*)···O(5)) to construct an infinite 1D chain, which are further arranged into 2D sheet through hydrogen bonds (Fig. 1b). The neighboring 2D sheets are connected through hydrogen bonds (O(6*w*)–H(6*wA*)···O(1)$^{\#2}$, O(5*w*)–H(5*wA*)···O(1), O(3*w*)–H(3*wA*)···O(4)$^{\#3}$, O(7*w*)–H(7*wB*)···O(5*w*)$^{\#4}$, O(6*w*)–H(6*wB*)···O(5)$^{\#5}$, O(3*w*)–H(3*wB*)···O(6*w*)$^{\#2}$, O(2*w*)–H(2*wA*)···O(3*w*)$^{\#7}$, O(1*w*)–H(1*wA*)···O(4*w*)) and π–π interactions (π–π interactions occur between the parallel pyridine rings of Phen with the centroid-to-centroid distances of 3.607 Å) to give rise to a supramolecular 3D framework (Figs. 1c and 1d). The corresponding data of hydrogen bonds are listed in Table 3.

Regarding to MOF **II**, the original ligand $H_2PZDA$ was decarboxylated in the form of HPZCA to form $[Cu(PZCA)_2(H_2O)_2] \cdot 2H_2O$ under hydrothermal conditions in the presence of $Cu^{2+}$ ion. MOF **II** gives a distorted octahedral geometry with N(1), O(1) and N(1*A*), O(1*A*) belonging to two molecules of PZCA ligand to occupy each vertex of the four equatorial sites, while two O atoms coming from two molecules of terminal water to locate in the apical positions along the axis (Fig. 2a). The corresponding bond angles are: O(1)Cu(1)N(1) 83.37°, O(1)Cu(1)N(1*A*) 96.65°, O(1*A*)Cu(1)N(1) 96.65° and O(1*A*)Cu(1)N(1*A*) 83.37)° (Table 2). The sum of bond angles is 360.00°, which indicates that the four atoms (O(1), O(1*A*), N(1) and N(1*A*)) are accurately coplanar under the experimental error. It also can be proved by the sum of the internal angle of the parallelogram (N(1)O(1)N(1*A*) 90.78°, O(1)N(1*A*)O(1*A*) 89.22°, N(1)O(1*A*)N(1*A*) 90.78° and O(1)N(1)O(1*A*) 89.22°, summation: 360.00°). Three diagonals defined by O(1)Cu(1)O(1*A*), O(1*w*)Cu(1)O(1*wA*) and N(1)Cu(1)N(1*A*) are exactly collinear. Among the bond lengths of Cu–O, Cu–O(*w*) and Cu–N, the lat-

**Table 3.** Geometric parameters of hydrogen bonds in MOFs **I** and **II***

| Contact D–H···A | Distance, Å | | | Angle D–H···A, deg |
|---|---|---|---|---|
| | D–H | H···A | D···A | |
| **I** | | | | |
| O(7*w*)–H(7*wA*)···O(5*w*)$^{\#1}$ | 0.85 | 1.97 | 2.812(3) | 169 |
| O(6*w*)–H(6*wA*)···O(1)$^{\#2}$ | 0.85 | 1.97 | 2.814(3) | 172 |
| O(5*w*)–H(5*wA*)···O(1) | 0.85 | 1.98 | 2.821(3) | 169 |
| O(4*w*)–H(4*wA*)···O(7*w*) | 0.85 | 1.97 | 2.798(3) | 163 |
| O(3*w*)–H(3*wA*)···O(4)$^{\#3}$ | 0.85 | 2.06 | 2.842(3) | 153 |
| O(7*w*)–H(7*wB*)···O(5*w*)$^{\#4}$ | 0.85 | 1.96 | 2.812(3) | 178 |
| O(4*w*)–H(4*wB*)···O(5) | 0.85 | 1.98 | 2.799(2) | 162 |
| O(6*w*)–H(6*wB*)···O(5)$^{\#5}$ | 0.85 | 1.95 | 2.793(2) | 172 |
| O(5*w*)–H(5*wB*)···O(8)$^{\#6}$ | 0.85 | 1.83 | 2.672(3) | 174 |
| O(1*w*)–H(1*wB*)···O(6) | 0.85 | 1.83 | 2.675(2) | 169 |
| O(3*w*)–H(3*wB*)···O(6*w*)$^{\#2}$ | 0.85 | 1.97 | 2.818(3) | 180 |
| O(2*w*)–H(2*wA*)···O(3*w*)$^{\#7}$ | 0.85 | 1.87 | 2.688(2) | 162 |
| O(2*w*)–H(2*wB*)···O(3) | 0.85 | 1.77 | 2.616(2) | 174 |
| O(1*w*)–H(1*wA*)···O(4*w*) | 0.85 | 1.90 | 2.692(2) | 155 |
| **II** | | | | |
| O(2*w*)–H(2*wB*)···O(2)$^{\#2}$ | 0.85 | 2.00 | 2.818(3) | 161 |
| O(2*w*)–H(2*wA*)···O(2)$^{\#3}$ | 0.85 | 2.01 | 2.834(3) | 163 |
| O(1*w*)–H(1*wB*)···N(2) | 0.85 | 2.38 | 3.182(3) | 157 |
| O(1*w*)–H(1*wA*)···O(2*w*)$^{\#4}$ | 0.85 | 1.88 | 2.732(3) | 177 |

* Symmetry transformations used to generate equivalent atoms: $^{\#1}$ $x-1, y, z$; $^{\#2}$ $-x+1, -y+1, -z+1$; $^{\#3}$ $x, y+1, z$; $^{\#4}$ $-x+1, -y+1, -z$; $^{\#5}$ $x, y, z+1$; $^{\#6}$ $x+1, y+1, z$; $^{\#7}$ $x, y-1, z$ (**I**); $^{\#1}$ $-x+1, -y+1, -z+2$; $^{\#2}$ $-x+1, -y+1, -z+1$; $^{\#3}$ $-x+1, y-1/2, -z+3/2$; $^{\#4}$ $x-1, y, z-1$ (**II**).

ter one is longest, probably due to the stronger bidentate chelating effect of PZCA ligand. The lengths of Cu–N, Cu–O and Cu–O(*w*) are consistent with those in the similar MOFs reported. Though the reported complexes are somewhat similar to MOF **II**, some differences also exist between them including crystallographic data, molecule weight, coordination environments of the central metal ions, etc. [22–24]. The discrete 0D units of MOF **II** connected into 1D chain via hydrogen bonds and π–π interactions and then linked into coplanar 2D sheet through hydrogen bonds (Figs. 2a and 2b), which are further assembled into 3D framework through hydrogen bonds bridged by the linkers of lattice water molecules (Fig. 2d). A fascinating and peculiar structural feature of MOF **II** exhibits the alternate arrangement of ring A and ring B motifs in the form of $(ABABAB)_\infty$ in the same plane to generate the porous 2D sheet (Fig. 2c), which present two kinds of opening porosities in the 3D architecture (Fig. 2d).

What's noteworthy is that HPZCA ligands derive from in situ decarboxylation of original $H_2PZDA$ ligands under hydrothermal conditions in the presence of $Cu^{2+}$ ion:

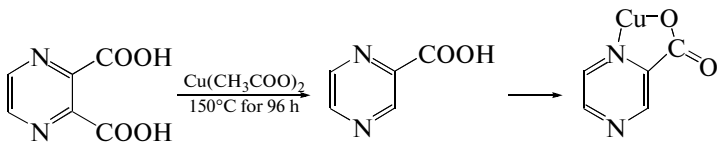

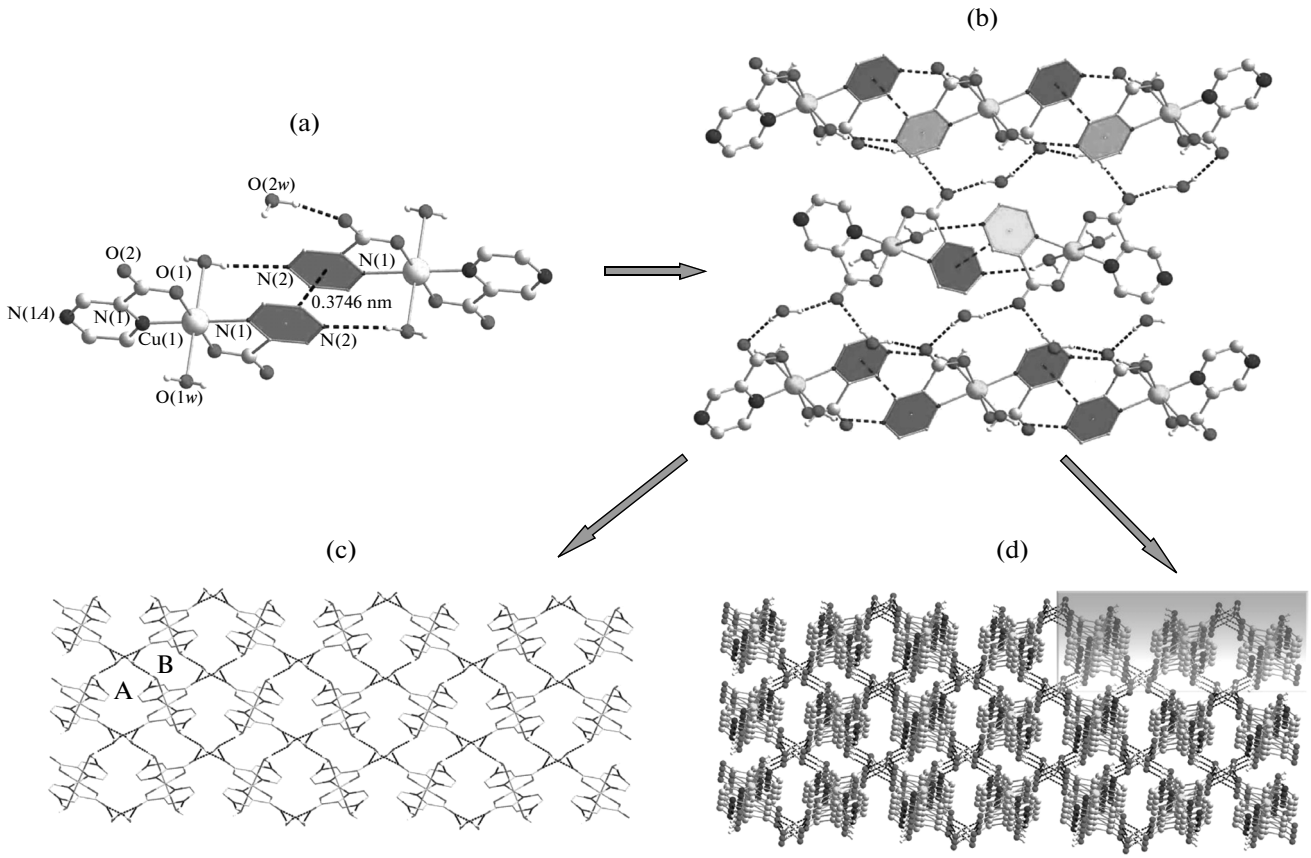


**Fig. 2.** The formation of 3D framework of $[Cu(PZCA)_2(H_2O)_2] \cdot 2H_2O$: coordination environment of the MOF **II** (a); view of the hydrogen bonds and π–π interactions in the 2D structure (b); view of the 2D single sheet linked via 1D chains (c); view of the 3D framework (d).

(only one of the carboxylates in $H_2PZDA$ ligand is decarboxylated). To make a further understanding of this kind of phenomenon, the comparative experiments have been performed. In the first experiment, the other reaction conditions were kept unchanged except the amount of $Cu^{2+}$ ion was doubled, the identical crystals were obtained. In the second experiment was made directly from $H_2PZDA$ ligand without $Cu^{2+}$ ion at 150°C (with other conditions were changeless), the HPZCA ligand could not be generated, namely, the in situ decarboxylations of $H_2PZDA$ ligands didn't occur. In the third experiment we attempted to synthesize MOF **II** by starting the reaction from HPZCA ligand in stead of $H_2PZDA$, however, the title MOF **II** could not be obtained. These results indicate that $Cu^{2+}$ ion may play a promotional role in decarboxylation in this reaction process at 150°C. Some similar results about in situ decarboxylations of multicarboxylic acid promoted by $Cu^{2+}$ ion have also been reported [25–28].

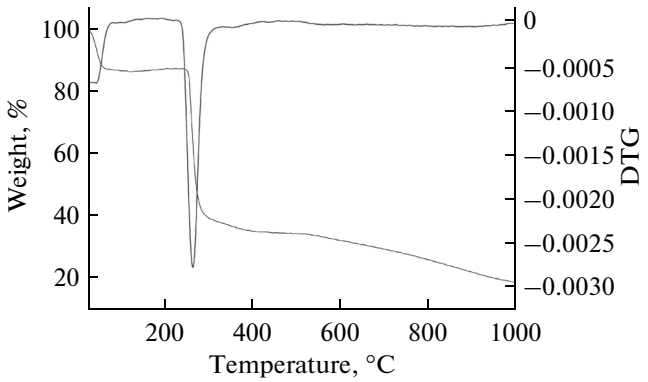


**Fig. 3.** TG–DTG curves of the MOF **I**.

The TG and DTG curves of the MOF **I** are shown in Fig. 3, which indicate that the MOF decomposes in two steps. The first weight loss stage has a decomposition temperature range of 25–100°C, with a weight loss of 13.41%, which corresponds to the loss of part of five molecules of coordinated water and two molecules of $H_2O$ ligands (theoretical loss is 13.36%). On further heating, the material loses weight continuously during the second step, which has a decomposition temperature range of 243–980°C, with a weight loss of 67.62%, corresponding to the loss of two molecules of Phen and two molecules of $H_2PDA$ ligands (theoreti-

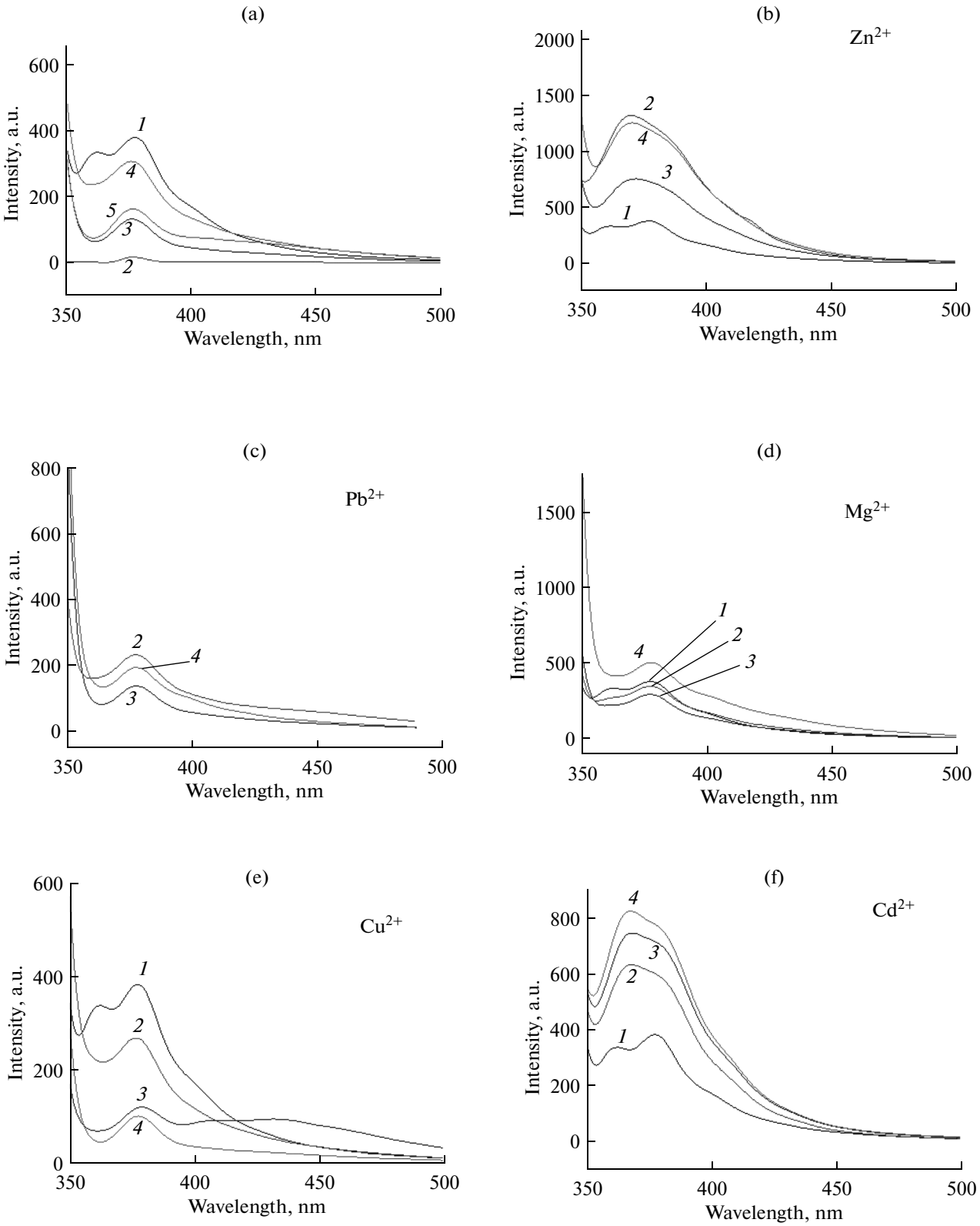


**Fig. 4.** Emission spectra of MOF **I** in methanol ($10^{-4}$ M) at room temperature ($\lambda_{ex}$ = 337 nm) in the presence of $Zn^{2+}$, $Cd^{2+}$, $Mg^{2+}$, $Pb^{2+}$, and $Cu^{2+}$ ions with respect to **I**: (a)—MOF **I** (*1*), methanol (*2*), $Cu(Ac)_2 \cdot H_2O$ (*3*), Phen (*4*), $H_2PDA$ (*5*) (concentrations of all compounds $10^{-4}$ M); (b)—$Zn^{2+}$, (c)—$Pb^{2+}$, (d)—$Mg^{2+}$, (e)—$Cu^{2+}$, (f)—$Cd^{2+}$ (no addition (*1*), 1 (*2*), 2 (*3*), 3 equiv (*4*)).

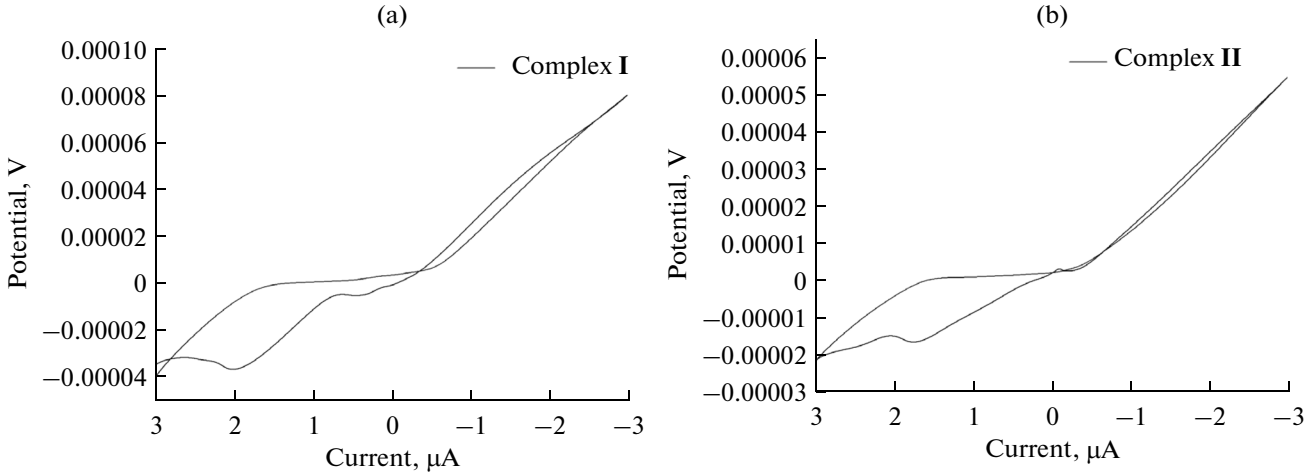


**Fig. 5.** Cyclic voltammograms of MOF **I** (a) and **II** (b) in methanol at $v = 0.25$ V/s.

cal loss is 69.35%). The fact that $H_2PDA$ ligands are lost at a higher temperature suggests that they are coordinated with the Cu atoms. The decomposition product is identified as CuO. The observed weight 18.97% is in agreement with the calculated value (17.29%).

The luminescent properties of MOF **I** are studied in methanol ($10^{-4}$ M) at room temperature. Emission spectra of MOF **I** (excited at 337 nm) in the presence of $Cd^{2+}$, $Cu^{2+}$, $Mg^{2+}$, $Pb^{2+}$, and $Zn^{2+}$ ions with respect to MOF **I** are listed in Fig. 4, respectively. MOF **I** exhibits intense broad emission bands at 362 and 377 nm, which may be due to the $\pi^* \rightarrow n$ or $\pi \rightarrow \pi^*$ transition. According to the above results, the emission of MOF **I** may be assigned to the ligand-to-metal-charge-transfer bands (LMCT). The emission intensity of MOF **I** increases signicantly upon adding $3 \times 10^{-4}$ mol $L^{-1}$ of $Cd^{2+}$ (from $Cd(Ac)_2$). The highest peak at 362 nm increased nearly three times as intense as the corresponding bands in the solution without adding. The highest peak at 362 nm for the MOF **I** was at least three times as intense as the corresponding bands in the solution without $1 \times 10^{-4}$ mol $L^{-1}$ of $Zn^{2+}$ and decreased to three times when $1 \times 10^{-4}$ mol $L^{-1}$ of $Pb^{2+}$. In contrast, the same experiments were performed with the introduction of $Mg^{2+}$. As a result, the metal ions have no significant effect on the luminescent intensities. The results above support the notion that the luminescent emission of MOF **I** display selectivity on a certain extent for $Zn^{2+}$, $Cu^{2+}$, $Pb^{2+}$, and $Cd^{2+}$.

The cyclic voltammograms graphics of MOF **I** and **II** in methanol ($10^{-4}$ M) solution are shown in Fig. 5. From 2 to 0 V, there are two irreversible oxidation peaks of the MOFs, one at the $E_{pa} = 387$ mV and the other at the $E_{pa} = 1997$ mV, which corresponding to the ligands and Cu(I)/Cu(II) oxidation process. There is one weak reduction peak at the $E_{pa} = 1591$ mV, which corresponding to ligands $PDA^{2-}$ and ligands reduction process. The electrochemical property of MOF **II** is similar to that of MOF **I** (Fig. 5).

## ACKNOWLEDGMENTS

This work was supported by the Natural Science Foundation of Henan Province, P.R. China (nos. 13A150056, 12B150005, 122102210174 and 12B150004).

## REFERENCES

1. Deng, H., Grunder, S., Cordova, K.E., et al., *Science*, 2012, vol. 336, no. 6084, p. 1018.
2. Wang, C., Zhang, T., and Lin, W., *Chem. Rev.*, 2012, vol. 112, no. 7, p. 1084.
3. Zhao, B., Gao, H.L., Chen, X.Y., et al., *Chem. Eur. J.*, 2006, vol. 12, no. 1, p. 149.
4. Devereux, M., McCann, M., Leon, V., et al., *Polyhedron*, 2002, vol. 21, no. 12, p. 1063.
5. Ramezanipour, F., Aghabozorg, H., Sheshmani, S., et al., *Acta Crystallogr., E*, 2004, vol. 60, no. 45, p. m1803.
6. Wen, G.L., Wang, Y.Y., Liu, P., et al., *Inorg. Chim. Acta*, 2009, vol. 362, no. 8, p. 1730.
7. Li, M., Xiang, J., Yuan, L., et al., *Cryst. Growth Des.*, 2006, vol. 6, no. 9, p. 2036.
8. Liu, M.S., Yu, Q.Y., Cai, Y.P., et al., *Cryst. Growth Des.*, 2008, vol. 8, no. 11, p. 4083.
9. Yang, L.R., Song, S., Shao, C.Y., et al., *Synth. Met.*, 2011, vol. 161, no. 4, p. 1500.
10. Yang, L.R., Song, S., Shao, C.Y., et al., *Synth. Met.*, 2011, vol. 161, nos. 11–12, p. 925.
11. Wang, Z. and Cohen, S.M., *Chem. Soc. Rev.*, 2009, vol. 38, no. 5, p. 1315.
12. Zhu, T., Ikarashi, K., Ishigaki, T., et al., *Inorg. Chim. Acta*, 2009, vol. 362, no. 1, p. 3407.
13. Zhao, B., Chen, X.Y., Cheng, P., et al., *J. Am. Chem. Soc.*, 2004, vol. 126, no. 47, p. 15394.

14. Brouca-Cabarrecq, C., Dexpert-Ghys, J., Fernandes, A., et al., *Inorg. Chim. Acta*, 2008, vol. 361, nos. 9–10, p. 2909.
15. Mahata, P., Ramya, K.V., and Natarajan, S., *Dalton Trans.*, 2007, no. 36, p. 4017.
16. Dossantos, C., Harte, A., Quinn, S., et al., *Chem. Rev.*, 2008, vol. 252, no. 18, p. 2512.
17. Matsuda, R., Kitaura, R., Kitagawa, S., et al., *J. Am. Chem. Soc.*, 2004, vol. 126, no. 43, p. 14063.
18. Sheldrick, G.M., *SHELXTL,Version 5, Reference Manual*, USA: Siemens Analytical X-ray Systems, 1996.
19. Premkumar, T., Govindarajan, S., Coles, A.E., et al., *J. Phys. Chem.*, *B*, 2005, vol. 109, no. 13, p. 6126.
20. Gabr, I.M., El-Asmy, H.A., Emmam, M.S., et al., *Transition Met. Chem.*, 2009, vol. 24, no. 32, p. 409.
21. Nakamoto K., *Infrared and Raman Spectra of Inorganic and Coordination Compounds*, New York: John Wiley and Sons, 1997.
22. Klein, C.L., Majeste, R.J., Trefonas, L.M., et al., *Inorg. Chem.*, 1982, vol. 21, no. 5, p. 1891.
23. Wang, G.H., He, R.L., Meng, F.J., et al., *Acta Crystallogr.*, *E*, 2009, vol. 65, p. m1511.
24. Chutia, P., Kato, S., Kojima, T., et al., *Polyhedron*, 2009, vol. 28, no. 10, p. 370.
25. Wu, W.P., Wang, Y.Y., Wu, Y.P., et al., *CrystEngComm*, 2007, vol. 9, p. 753.
26. Frisch, M. and Cahill, C.L., *J. Solid State Chem.*, 2007, vol. 180, no. 36, p. 2597.
27. Ziegelgruber, K.L., Knope, K.E., Frisch, M., et al., *J. Solid State Chem.*, 2008 vol. 181, no. 8, p. 373.
28. Zhong, D.C., Lu, W.G., Jiang, L., et al., *Cryst. Growth Des.*, 2009, vol. 10, no. 2, p. 739.